

Effect of retinol dehydrogenase gene transfer in a novel rat model of Stargardt disease

T. Cronin, Mikael Croyal, N. Provost, J. Ducloyer, A. Mendes-Madeira, L. Libeau, C. Morival, E. Toublanc, C. Audrain, C. Isiegas, et al.

▶ **To cite this version:**

T. Cronin, Mikael Croyal, N. Provost, J. Ducloyer, A. Mendes-Madeira, et al.. Effect of retinol dehydrogenase gene transfer in a novel rat model of Stargardt disease. FASEB Journal, 2021, 35 (11), pp.1-17. 10.1096/fj.202002525RRR . hal-03793154

HAL Id: hal-03793154
https://hal.inrae.fr/hal-03793154

Submitted on 30 Sep 2022

HAL is a multi-disciplinary open access archive for the deposit and dissemination of scientific research documents, whether they are published or not. The documents may come from teaching and research institutions in France or abroad, or from public or private research centers.

L'archive ouverte pluridisciplinaire **HAL**, est destinée au dépôt et à la diffusion de documents scientifiques de niveau recherche, publiés ou non, émanant des établissements d'enseignement et de recherche français ou étrangers, des laboratoires publics ou privés.



Distributed under a Creative Commons Attribution 4.0 International License

Received: 30 November 2020 | Revised: 25 August 2021 | Accepted: 3 September 2021

DOI: 10.1096/fj.202002525RRR

THE FASEB JOURNAL

RESEARCH ARTICLE

Effect of retinol dehydrogenase gene transfer in a novel rat model of Stargardt disease

T. Cronin[1] | **M. Croyal**[2] | **N. Provost**[1] | **J. B. Ducloyer**[3] | **A. Mendes-Madeira**[1] | **L. Libeau**[1] | **C. Morival**[1] | **E. Toublanc**[1] | **C. Audrain**[1] | **C. Isiegas**[1] | **V. Pichard**[1] | **O. Adjali**[1]

[1]Université de Nantes, CHU de Nantes, INSERM UMR 1089, Translational Gene Therapy for Genetic Diseases, Nantes, France

[2]Inserm UMR1280, Nantes, France

[3]Department of Ophthalmology, University Hospital of Nantes, CHU de Nantes, Nantes, France

Correspondence
T. Cronin and O. Adjali, IRS 2 Nantes Biotech - Université de Nantes, 22 Boulevard Benoni Goullin, F-44200 Nantes, France.
Email: therese.cronin@univ-nantes.fr (T. C.) and oumeya.adjali@univ-nantes.fr (O. A.)

Funding information
Aviesan/Unadev, Grant/Award Number: 19UU50; Connect Talent 2015 (Pays de la loire)

Abstract

Dysfunction of the ATPase-binding Cassette Transporter protein (ABCA4) can lead to early onset macular degeneration, in particular to Stargardt disease. To enable translational research into this form of blindness, we evaluated the effect of Cas9-induced disruptions of the ABCA4 gene to potentially generate new transgenic rat models of the disease. We show that deletion of the short exon preceding the second nucleotide-binding domain is sufficient to drastically knock down protein levels and results in accumulation of retinoid dimers similar to that associated with Stargardt disease. Overexpression of the retinol dehydrogenase enzymes RDH8 and RDH12 can to a limited extent offset the increase in the bis-retinoid levels in the *Abca4*$^{Ex42-/-}$ KO rats possibly by restricting the time window in which retinal can dimerize before being reduced to retinol. However, in vivo imaging shows that overexpression of RDH8 can induce retinal degeneration. This may be due to the depletion in the outer segment of the cofactor NADPH, needed for RDH function. The translational potential of RDH therapy as well as other Stargardt disease therapies can be tested using the *Abca4* knockdown rat model.

KEYWORDS

ABCA4, NADPH, retinoid toxicity, retinol dehydrogenase, Stargardt disease, transgenic rat

1 | INTRODUCTION

Photoreceptor cells in the mammalian retina detect and absorb photons of light enabling vision. This light absorption takes place on the membrane of the apical segments or 'discs' of photoreceptors and is mediated by retinal in covalent linkage with the apoprotein opsin. One adaptation of the photoreceptor is the recruitment of a flippase transporter on the membrane to clear accumulated retinal from the lumenal space within these discs to the photoreceptor

Abbreviations: ABCA4, ATPase-binding cassette transporter; *at*Ral, all-*trans* retinal; *at*Rol, all-*trans* retinol; Cas9, CRISPR-associated protein 9; ERG, electroretinogram; OCT, optical coherence tomography; POS, photoreceptor outer segment; rAAV, recombinant adeno-associated virus; RDH, retinol dehydrogenase; STGD1, Stargardts disease.

This is an open access article under the terms of the Creative Commons Attribution-NonCommercial-NoDerivs License, which permits use and distribution in any medium, provided the original work is properly cited, the use is non-commercial and no modifications or adaptations are made.
© 2021 The Authors. *The FASEB Journal* published by Wiley Periodicals LLC on behalf of Federation of American Societies for Experimental Biology

cytosolic space where it can safely be incorporated into the retinoid metabolic cycle. The gene encoding this flippase, the ATPase-binding Cassette Transporter (ABCA4), has been fully characterized by the accumulated work of a few research groups.[1-4] Despite a modest role in vision, the consequences of ABCA4 dysfunction are profound and can lead to Stargardt disease (STGD1) and some forms of cone-rod dystrophy for which effective treatments are not yet currently available.[4–7] These pathologies stem from the high reactivity of retinal, which is necessary to trigger the photochemical reaction that facilitates vision but also poses a potential hazard for the photoreceptor cell. Retinal, in addition to forming a Schiff base on rhodopsin, can react with any primary amine, of which there are an abundance in the phospholipid-rich photoreceptor membranes.[8] The intermediates that result can react with another retinal leading to dimers, termed bisretinoids, of differing isomers whose toxicity to the mammalian cell has been extensively described.[9–15] When not sequestered with opsin to mediate vision, retinal must therefore be reduced to a less reactive form. This occurs early in the visual cycle, a series of enzymatic reactions that recycle retinal from the 'bleached' *trans* isomer all-*trans* retinal (*at*Ral) to a 'receptive' *cis* isomer (11*cis*RAL) for continued photon absorption.[16–18] The reduction of *at*Ral to the less reactive alcohol form retinol (*at*Rol) is carried out by the retinol dehydrogenase enzyme RDH8 and supported by RDH12.[19–21] However, an estimated 24% of *at*Ral escapes this reduction reaction and reversibly reacts with phosphatidylethanolamine (PE) in disc membranes to form *N*-retinylidene-PE.[22] This is particularly likely to occur with the passive diffusion of *at*RAL into the lumen of the photoreceptor disc where RDH is size-excluded. ABCA4 plays an essential role in minimizing dimerization of *at*RAL. It achieves this by catalyzing the 'flip' of retinal and *N*-retinylidene-PE from the lumen of the multiple stacked photoreceptor discs to the cytosol where it is released by ATP and can be reduced by the RDH8 enzyme.

The pathophysiology of STGD1 has been unraveled over the past two decades using pigmented and non-pigmented STGD1 mouse models. This, despite the fact that rodents lack a macula and ABCA4 dysfunction is found to have little impact on functional rodent vision.[22] In these rodent models for instance, progressive lipofuscinogenesis, known in patients to precede retinal cell death, is shown to be driven by the accumulation of a heterogeneous bisretinoid mix, for which A2E is best characterized.[11,15] Reversing this biochemical signature has been a goal for initial screening of STGD1 therapies. These therapeutic strategies need to be innovative as ABCA4 is too large for the most commonly used recombinant Adeno-Associated Virus-derived vector systems (rAAV) complicating efforts to directly replace the gene. It also has over 1000 causal mutations limiting the benefits of a targeted gene correction. However, considerable recent progress has been made to treat STGD1 using dual AAV vectors expressing ABCA4 as well as using visual cycle modulators to reduce these bisretinoid biomarkers.[23–27] To further facilitate such early-stage biomedical research, we are developing rat *Abca4* mutant models through targeted mutations in the *Abca4* gene using a Cas9-based platform. There are advantages to developing rat STGD1 models for small animal modeling in retinal diseases. Firstly, subretinal injections in the mouse eye offer limited control over how much of the injected fluid is retained in the subretinal space without leaking to the vitreous or choroid. In the rat, the ocular membranes are more resistant allowing greater control using a stereotactic apparatus and reducing the risk of leak in the hour proceeding injection. Secondly, complications of prolonged *in vivo* retinal imaging arise in the anaesthetized mouse where opacity of the lens can develop quickly and compromise a full fundus imaging protocol, particularly in the immature animal. This effect caused by drying of the cornea as well as pseudo-cataract formation under anesthesia is present in most mouse models but does not arise in our experience with the rat.

To aid our early-stage testing of STGD1 therapeutic tools, we have developed and phenotyped STGD1 rat models using CrispR-Cas9 and single-stranded oligodinucleotides (ssODNs), as described by Remy and colleagues.[28] Rat zygotes that did not receive a ssODN showed NHEJ events in the *Abca4* gene that in some cases resulted in non-translation of stable protein. In this report we describe the phenotype of one such ABCA4 knockdown rat model and its similarity to STGD1 mouse models using the template proposed by Wilner in which the validity of an animal model for a disease is assessed by three criteria: Face, Construct and Predictive validity.[29] We also wished to examine whether overexpression of photoreceptor RDH enzymes may delay bisretinoid accumulation. The reduction step is a potential bottleneck in the visual cycle so it was of interest to see the effect of exogenous rAAV-mediated expression of RDH transgenes in these retinas.[30] We report that while this strategy can reduce bisretinoid levels in this rat model, the retinal tissue overexpressing RDH8 transgene shows signs of degeneration while being less impacted by RDH12 transgene. While RDH supplementation may have limited therapeutic potential the predictive validity of this new rat model for therapeutic testing is shown.

2 | MATERIALS AND METHODS

2.1 | Animals

The Transgenic Rat Platform at the University of Nantes (INSERM UMR 1064) generated the rats used in this study. The sgRNAs targeting exon 41 of the rat Abca4

gene were initially screened in rat C6 glioma cells before the following sgRNA sequence was selected, CCTCCAGTCCAGCAGTAGAT. Animals were maintained at the Boisbonne Centre (ONIRIS, Nantes-Atlantic College of Veterinary Medicine, Food Science and Engineering, Nantes, France) under a 12/12-h light/dark cycle. All experiments involving animals were conducted in accordance with the Association for Research in Vision and Ophthalmology statement for the use of animals in ophthalmic and vision research. Colony production and treatment protocols were approved by the Animal Experimentation Ethics Committee of the Pays de Loire (France) and the Ministère de l'Enseignement Supérieur et de la Recherche (APAFIS permit numbers 9639 and 16586). Genotyping is described in Supplementary methods. For all experiments rats were euthanized by intracardiac injection of sodium pentobarbital (Vealtoquinol, Lure, France) following inhalation of isofluorane gas.

2.2 | Electroretinography and FO-OCT

After overnight dark-adaptation, rats were sedated by gas anesthesia followed by ketamine intramuscular injection (Rompun® 2% − Imalgène 1000) and maintained by inhalation of isofluorane gas. Electroretinogram (ERG) were recorded bilaterally with contact lens electrodes following pupil dilation (Tropicamide, Novartis) and local anesthesia (Chlorhydrate oxybuprocaine, Théa, France). Up to 10 stimulations were carried out at each intensity of flash to obtain the stabilized measure. In vivo imaging was performed one week before each ERG using the Spectralis® HRA + optical coherence tomography (OCT) imaging system (Heidelberg Engineering Inc.) which combines simultaneous reflectance fundus imaging with OCT, and allows repeatable scanning at the same retinal region during follow-up studies. Contact lenses were not used for this imaging and the camera did not have an internal calibrator for fundus acquisition. Animals were placed on an adjustable platform, and the camera aligned perpendicular to the animal directly in front of the eye. The NIR reflectance mode in fundus imaging using the 820 nm laser was used for alignment and to ensure equivalent illumination over the 55° acquisition field for each animal. Images were recorded in automatic real time mode. A quantitative gray-level analysis of the fundus scans was performed using Fiji software as described previously.[31] With the exception of injected retinas, imaging was carried out in a mid-peripheral region superior to the optic disc. The gray value on unprocessed images was determined in this region of interest (ROI) using a plot profile on the thresholded image with subtraction of values for images taken without laser acquisition. The same area and pixel-radius, accessed from Fijis ROI manager, was used for each image. For OCT once the optic disc was centered and in focus using infrared imaging, the retina was covered by 30° horizontal B-scans with an average of 25 line scans using the high-resolution mode. For phenotyping, scans were made through the optic nerve head in the central superior retina. By contrast, for pre- and post-injection comparisons a fixed location in the peripheral superior retina where the injection is localized was scanned. During recordings, the cornea was kept lubricated; and during acquisition, image quality was determined by the quality signal index of the Spectralis software as well as the subjective assessment of the examiner.

2.3 | Mass spectrometry analyses

All solvents were LC-MS grade and purchased from Biosolve (Valkenswaard, Netherlands) unless otherwise specified. Rats were euthanized under dim red light and eye cups extracted in the dark, snap frozen in light-safe eppendorfs and stored at −80°C for further processing. A 2:1 methanol/chloroform mix was added to the frozen eyecups with retinyl acetate as an internal standard. Two sterile metal beads were added to each tube and the sample homogenised for 2 min using a tissuelyser (Qiagen, Hilden, Germany). The mouse eyes used as reference control were handled similarly with two eyecups analyzed per sample. Following 10-min centrifugation at 20 000 *g* the supernatants were transferred to screw-top glass vials and all solvent removed under a gentle stream of nitrogen. The dried samples were solubilized in a mixture of isopropanol/acetonitrile/water (50:25:25, v:v:v, 100 μl) prior mass spectrometry analyses. Liquid chromatography-high resolution mass spectrometry (LC-HRMS) analyses were performed on a Synapt™ G2 HRMS Q-TOF mass spectrometer equipped with an electrospray ionization interface operating in the positive mode and an Acquity H-Class® UPLC™ device (Waters Corporation, Milford, MA, USA). Samples were injected (10 μl) onto an Acquity® Charge Surface Hybrid C_{18} column (2.1 mm × 100 mm, 1.7 μm; Waters Corporation) held at 55°C. The mobile phase was composed of an acetonitrile/water (60:40, v:v) mixture as solvent A and an isopropanol/acetonitrile (90:10, v:v) mixture as solvent B, each containing 10 mmol/L ammonium acetate and 0.1% formic acid. The elution was carried out using a multistep gradient of solvent B in solvent A over 22 min at a constant flow rate of 400 μl/min. The elution started at 40% solvent B, followed by a linear gradient up to 43% solvent B over 2 min. Solvent B was immediately increased up to 50%, and ramped up to 54% over 10 min. Next, solvent B was increased to 70%, then ramped to 99% over 6 min,

and maintained at 99% for 2 min. The eluent composition returned to the initial conditions, and the LC column was equilibrated for 2 min prior the next injection. The full-HRMS mode was applied for detection (mass-to-charge ratio [*m/z*] range 50–1200) at a mass resolution of 30 000 full-widths at half maximum. The ionization settings were as follows: capillary voltage, +2 kV; cone voltage, 30 V; desolvation gas (N_2) flow rate, 900 L/h; desolvation gas/source temperatures, 550/120°C. Leucine enkephalin solution (2 μg/ml, 50% acetonitrile) was infused at a constant flow rate of 10 μl/min in the lockspray channel, allowing for correction of the measured *m/z* throughout the batch (theoretical *m/z* 556.2771 in positive mode). Data acquisition and processing were achieved using MassLynx® and TargetLynx® software (version 4.1, Waters Corporation). Biomarkers were extracted from the detected variables using their exact mass measured ±5 ppm, elemental compositions, retention times in comparison to reference standards, fragmentation patterns. Extracted ion chromatograms were obtained at *m/z* ratio of 592.4618, 746.4550, 551.4253, 836.5225, 792.5538, 740.5225 and 329.2481 for A2E, A2GPE, *at*RAL PE (22:6/22:6), PE (18:0/22:6), PE (18:2/18:2) and retinyl acetate, respectively. Chromatographic peaks were then integrated and normalized with that of internal standard. For Figure 3H the absolute levels of A2E were determined from standard curve for synthetic A2E resuspended in methanol. The purity of the final compound, generated by Atlanchim Pharma was 92.3% as determined by HPLC.

2.4 | Recombinant AAV vectors and subretinal injections

Expression cassettes included in the plasmid vectors used for the production of the rAAV2/5 vector were cloned using synthesized gene fragments (Integrated DNA Technologies, Belgium) containing the coding sequence for NM_015725.4 and NM_152443.3. The rAAV2 vectors were produced as previously described (Rabinowitz and Rolling, 2002) at the Vector Core facility of the University of Nantes (CPV-vector core, https://umr1089.univ-nantes.fr/facilities-cores/). The titer of rAAVs were determined using dot-blot and by transgene qPCR. For subretinal injections, rats were anaesthetised by inhalation of 5% isofluorane gas followed by IM injection of ketamine/xylazine (Imalgène1000/Rompun2%). Under an operating microscope, a transcleral/transchoroidal tunnel was carried out using surgical nylon suture (Ethilon 10/0) and the rAAV was delivered to the subretinal space using a 33G needle on a 5 ml Hamilton syringe. The stereotactic injection was performed at a rate of 2 μl/min. Up to 2.5 μl volume was injected with 1/1000 of fluorescein dye to monitor the bleb size. The relative success of the injection was evaluated by the size of bleb determined by OCT imaging immediately after injection.

2.5 | Western blot and immunohistochemistry

2.5.1 | Western blot

Samples (retinas) for Western blot analysis were lysed in SIE buffer (250 mM sucrose, 3 mM imidazole pH 7.4, 1% ethanol, and 1% NP-40, protease inhibitor) to extract ABCA4 protein. After lysis, ABCA4 samples were denatured at 37°C for 15 min in 1× Laemli sample buffer supplemented with 4 M urea. For The antibodies used for immuno-blotting are as follows: monoclonal anti-ABCA4 3F4 (1:500, RRID:AB_1118540), monoclonal anti-ABCA4 5B4 (1:500, MABN2440, Sigma Aldrich), monoclonal anti-β-actin (1:2000, RRID:AB_476744), monoclonal anti-GAPDH (1/1000, RRID:AB_1078991). For membrane separation, the Mem-Per Plus kit was used according to manufacturers instructions (Thermofisher, 89842).

2.5.2 | Immunohistochemistry

After euthanasia rat eyes were immediately enucleated and fixed for 5 h in Bouin's solution, dehydrated for 5 days and embedded in paraffin. Retinas were cut into 5-μm sections that were then deparaffinized and rehydrated for staining. Morphological analysis was performed after hematoxylin and eosin staining. Nuclei were counterstained with Mayer's hemalun solution and the slides were mounted and examined using a laser scanning confocal microscope (Nikon A1RSi). For flat-mount retinas, a mixture of anti Red/Green opsin (1/300, RRID:AB_177456) and Blue opsin (1/300, RRID:AB_177456) followed by 546-conjugated anti-rabbit IgG antibody (1/300; A.11010, Life Technologies) and draq5 (1/500, Biostatus Cat# DR50050, RRID:AB_2314341) counterstaining was used. Images were processed using Fiji (http://fiji.sc).

2.6 | qPCR expression

Most gene expression analyses were carried out using individual primers and Sybr green assays (Applied Biosystems) from which relative quantity (RQ) of transcript was determined. The RQ ($2^{-\Delta\Delta CT}$) was obtained in the test sample relative to the calibrator sample by normalizing C_T values for the gene of interest to the C_Ts for the two house-keeping genes, *Hprt* and *Tbp*. Relative

expression levels for rat glycolytic genes were determined using a custom-designed panel for PCR prime assay (https://www.bio-rad.com/en-us/prime-pcr-assays/select-plate-template) on a Biorad CFX96 machine. The array was designed on the Biorad website by modifying a predesigned array for glyocolysis/gluconeogenesis pathway for mouse (https://www.bio-rad.com/fr-fr/prime-pcr-assays/predesigned-plate/sybr-green-glycolysis-gluconeogenesis-m96). For those primer pairs not selected from Biorad PrimePCR validated list, the efficiencies were determined by a 6-point standard curve and incorporated into the analyses according to the template described by Pfaffl.[32]

2.7 | Statistical methods

Statistical analyses were performed using GraphPad Prism version 8.0.0 (GraphPad Software, San Diego, California USA). For most figures the data were passed for normality (Shapiro–Wilk) before analysis. An exception was the RT-qPCR data of Figure 1C and outer nuclear layer (ONL) counts of Figure 2B, which had too low a sample number ($n = 3$) for accurate normality distribution testing and were analyzed by Wilcoxon signed-rank test. ANOVA and regression analysis was used to compare ERG amplitude and OCT differences in genotypes with age. All other data were analyzed by Kruskal-Wallis test of variance or a two-tailed unpaired *t*-test. p value $<.05$ was considered statistically significant.

3 | RESULTS

3.1 | Maintenance of function with retinal thinning in the *Abca4*$^{Ex42-/-}$ transgenic rat

The rat *Abca4* gene was targeted for disruption by SpCas9 RNP microinjection into the pronucleus of intact rat zygotes and screened for NHEJ events on the gene. The sgRNA was designed to guide the nuclease to exon 41 of *Abca4* where end-joining led to sequence deletion (Figure 1A). This region was targeted to induce changes in or close to the nucleotide-binding domain 2 (NBD2) domain, where frequent mutations arise in STGD1 patients.[33] Two albino Sprague-Dawley rat transgenic lines, carrying 85 and 133-bp gene deletions were analyzed. Sequencing of cDNA for both lines shows the deletions resulted in the same splicing-mediated loss of a conserved region for ABC transporters at the start of NBD2. The incorrect splicing of a donor site from intron 41 to a splice-acceptor site from intron 42 resulted in loss of exon 42 while maintaining the correct reading frame. Despite the loss of exon 42 the levels of r*Abca4* transcript are not significantly altered as determined by RT-qPCR on the retinal RNA (Figure 1B). However, unexpectedly, the loss of the 21 amino acids of exon 42 is sufficient to result in a significant knockdown of *ABCA4* protein as observed in retinal lysates from the mutant rat retinas probed with monoclonal antibodies against the N- and C-terminals of the protein (Figure 1C). Both the 5B4 and 3F4 clones do not detect protein after 1 min of exposure (top and second western blot strips) with the protein in the WT sample banding as a doublet between 238 and 268 kDa. When the blots are left to over-expose for 15 min, protein in the mutant lysates is picked up, though only by the 3F4 clone (third western blot strip of 1C). This suggests that residual protein is present albeit at much diminished levels such that the WT protein saturates at the exposure lengths needed to reveal the mutant band (the original blots are shown in Figure S1). Quantification of the level of protein in Figure 1D is based on the 15-min exposure signal from the 3F4 antibody. It shows the model to be a hypomorphic rather than a true knockout with 88% reduction in the level of protein. As the protein was only weakly detected by western blot, the model is referred to from herein as *Abca4*$^{Ex42-/-}$. To further investigate the residual protein in the mutant rat retinas the protein extraction was carried out so as to separate membrane and cytosolic fractions. From this it is clear that much of the residual protein in the mutant retinas is aberrantly localized to the cytosol while only an estimated 4%–6% of the WT protein remains in the cytosol (Figure 1E,F). The persistence of *Abca4* gene transcripts (Figure 1B) suggests protein is lost through a post-translational degradation with some protein escaping in the cytosol, as has been similarly described in a recent Abca4 mutant mouse model.[34] The loss of Abca4 protein does not cause imbalance in the expression of other visual cycle genes (Figure S2). Non-invasive in vivo imaging by OCT was carried out at spaced time-points to see how the retinal structure changed with age. These analyses show a 28% reduction in the rat *Abca*$^{Ex42-/-}$ ONL by 12 months of age (Figure 2A). The difference is confirmed upon paraffin embedding of the retinas at the end of the study and counting the nuclei across 5 evenly spaced sections where a 30% reduction in cell number for the ONL is determined in the *Abca4*$^{Ex42-/-}$ eyes compared to WT (Figure 2B). However, L/M and S-opsin counts in the flat-mounted retinas are unchanged at 12 months of age showing cones to be unimpacted in this rat model (Figure S2).

The ERG, measuring the amplitude of the voltage response across the cornea to flashes of defined light intensity is a commonly used measure of retinal function. In transgenic rats, the follow-up was repeated over several time-points as the rats age using flashes of incrementally increasing intensity on the dark-adapted retina. Amplitude responses to

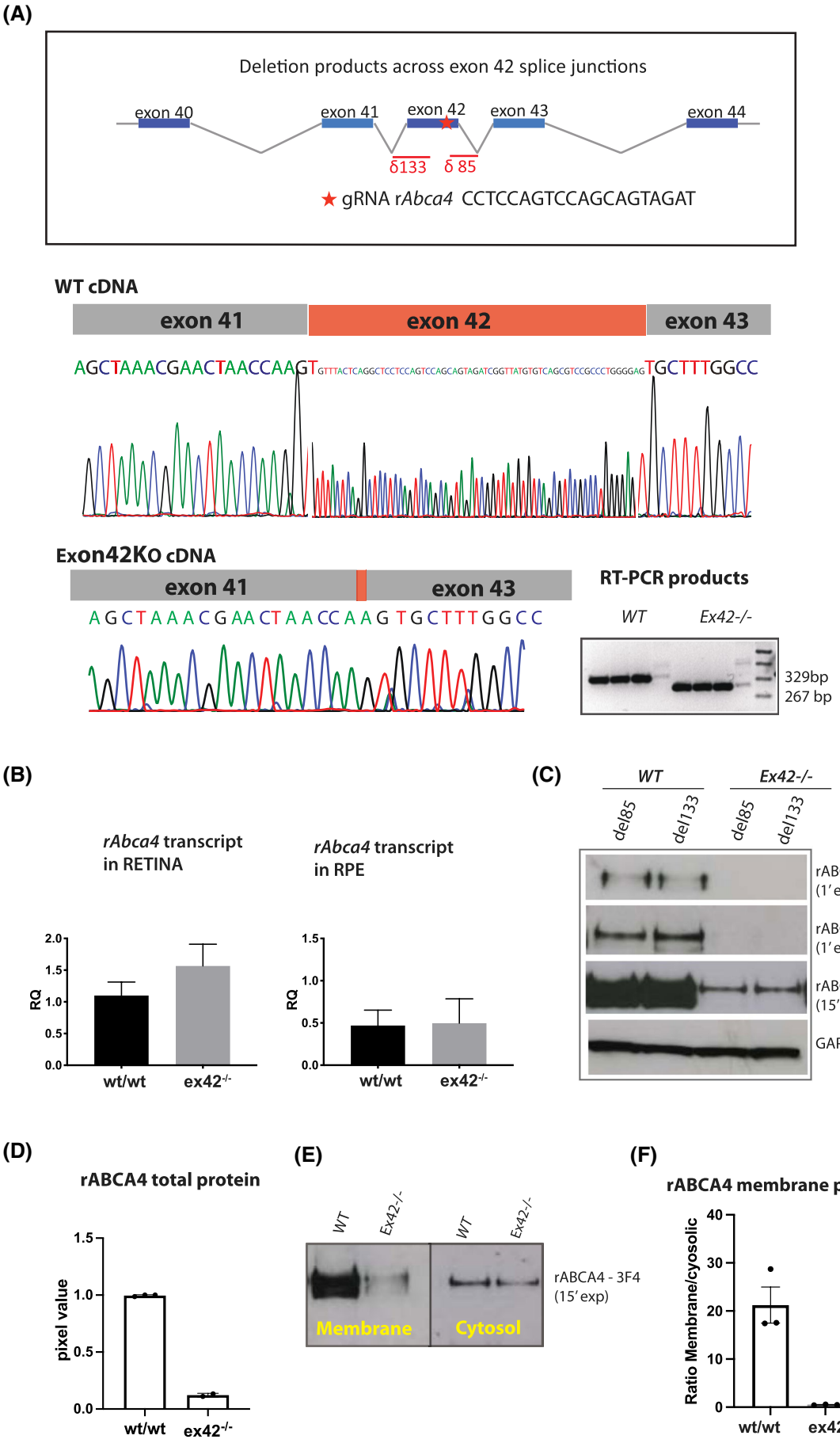
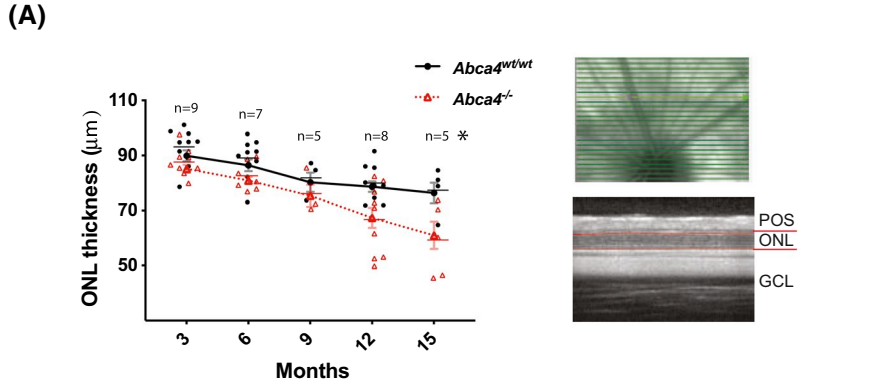

(A)
Deletion products across exon 42 splice junctions
exon 40
exon 41
exon 42
exon 43
exon 44
δ133
δ 85
★ gRNA rAbca4 CCTCCAGTCCAGCAGTAGAT
WT cDNA
exon 41
exon 42
exon 43
AGCTAAACGAACTAACCAAGT
TGCTTTGGCC
Exon42KO cDNA
exon 41
exon 43
AGCTAAACGAACTAACCAAG TGCTTTGGCC
RT-PCR products
WT
Ex42-/-
329bp
267 bp
(B)
rAbca4 transcript in RETINA
rAbca4 transcript in RPE
RQ
2.0
1.5
1.0
0.5
0.0
wt/wt
ex42-/-
(C)
WT
Ex42-/-
del85
del133
del85
del133
rABCA4 - 5B4 (1'exp)
rABCA4 - 3F4 (1'exp)
rABCA4 - 3F4 (15'exp)
GAPDH
(D)
rABCA4 total protein
pixel value
1.5
1.0
0.5
0.0
wt/wt
ex42-/-
(E)
WT
Ex42-/-
WT
Ex42-/-
Membrane
Cytosol
rABCA4 - 3F4 (15'exp)
(F)
rABCA4 membrane protein
Ratio Membrane/cytosolic
40
30
20
10
0
wt/wt
ex42-/-

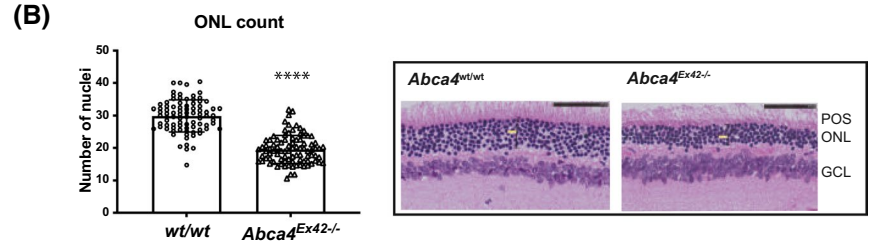
FIGURE 1 Generation of two Abca4 knockout transgenic rat lines. (A) A gRNA targeting exon 42 at the start of the second nucleotide binding domain of the rat *Abca4* gene was used to disrupt the *Abca4* coding sequence leading to two NHEJ products: one containing a 85 bp deletion and a second containing a 133 bp deletion. Both genome deletions led to the same *Abca4* transcript product with exon 42 removed in the rat mRNA as shown by sequencing of RT-PCR products 'WT cDNA' and 'Exon42KO cDNA' in this region. (B) RT-qPCR on retinal RNA from the mutant rats shows the deletion of exon 42 does not impact the RNA expression level of *Abca4* with a non-significant increase of expression in the retina and a low level of expression in the RPE, $n = 3$. (C) Retinal lysates from *Abca4-Ex42*$^{\delta 85/\delta 85}$ and *Abca4-Ex42*$^{\delta 133/\delta 133}$ rats and WT non-affected siblings, $n = 3$, were tested by western blot using monoclonal antibodies to epitopes in the N-terminal domain (5B4) and C-terminal domain (3F4). Both antibodies show absence of the target protein after 1 min of exposure time (first and second strips of the western blot). However, where the C-terminal 3F4 blot was left to expose for 15–18 min a band appears at the expected 268 kDa size of *ABCA4* (third strip). This suggests a residual amount of protein is present for both deletion strains. No additional protein products were identified as shown in the uncropped image of the western blot membrane (Figure S1). (D) The targeted disruption results in an estimated 88% knock-down on ABCA4 total protein level, $n = 3$, as measured by densitometry from the 15-min exposed bands. (E) Protein extracts were prepared with the separation of membrane and cytosolic fractions and the lysates probed with the 3F4 antibody (two separate extraction experiments on $n = 4$ rats). Blots were left to overexpose for 15 min showing the residual *ABCA*4 protein in the rats with the exon-42 deletion to be retained in the cytosol. With high resolution gels, the 3F4 antibody reveals a doublet banding between 220 and 268 kDa. In the cytosolic fraction the upper molecular weight band (between 250 and 268 kDa) predominates over the lower molecular weight band (between 220 and 250 kDa). (F) The ratio of the intensity of membrane/cytosolic protein bands was determined showing 20-fold increased concentration of *ABCA4* protein at the membrane compared to protein trapped in the cytosol in the WT retinas. By contrast, only a fraction of the residual protein in the retinas carrying exon-42 deletion reaches the cytosol. GCL, ganglion cell layer; gRNA, guide RNA; INL, inner nuclear layer, NHEJ, non homologous end-joining; ONL, outer nuclear layer; POS, photoreceptor outer segment; RQ, relative quantity

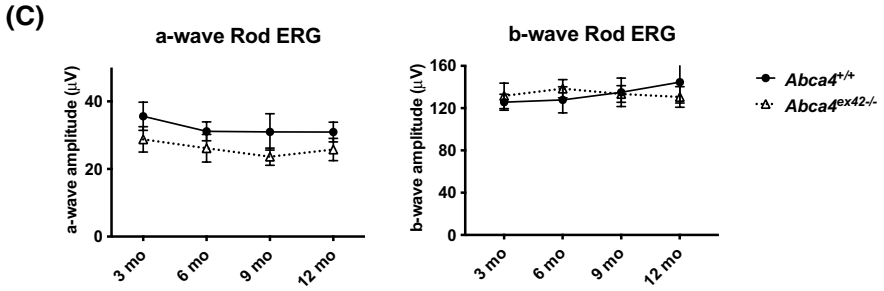
flashes that stimulate only-rod photoreceptors rod-cone mix and only-cones are not significantly changed at each age group compared to WT with 5 rats also followed over time (Figure 2C–E). We also note no difference in the kinetics of rod recovery following saturating flash in the rats tested at 6 months of age (Figure 2F) as distinct from that described for the well-described *Abca4*KO mouse ERG.[35,36] A possible consequence of the ONL thinning at 12 months of age may be reflected by the drop in the amplitude responses in the mixed rod-cone ERG, however we note that the amplitudes at these later ages do show more variability (Figure 2D). As well as cell loss, ONL thinning may arise with remodeling of the retina, a phenomenon described for a number of RD models.[37] While such remodeling is typically considered maladaptive, recent studies have shown that it may aid the degenerating retina to maintain normal overall retinal function even as photoreceptor input is impacted.[38,39] This reorganization supports signal compensation at the first synapse so as to maximize bipolar cell output relative to photoreceptor input. We find in this rat model that a shift occurs when the log of bipolar cell amplitude responses (log b-wave) are plotted as a function of photoreceptor amplitude responses (a-wave) with maximal bipolar cell responses being achieved at lower photoreceptor amplitudes (Figure S3). Irrespective of ONL thinning, the retinal ERG function in the *Abca*$^{Ex42-/-}$ rats is minimally impacted by the loss of ABCA4.

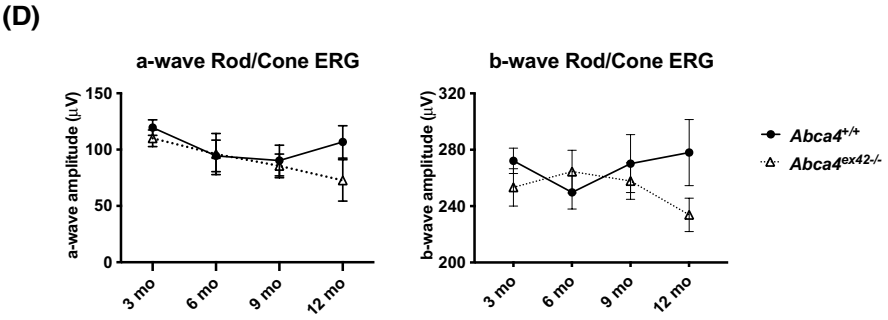
3.2 | Increase in bisretinoid levels in the *Abca4*$^{Ex42-/-}$ transgenic rat

In the case of dysfunction of ABCA4 protein, *N*-all-trans- and *N*-11cis-retinylidene-PE molecules accumulate in the lumen of the photoreceptor outer segment (POS). Dimerization will lead to the formation of N-Retinylidene-N-Retinyl-Phosphatidylethanolamine (A2PE) that will be further processed in the RPE phagosomes following POS engulfment by the Retinal Pigment Epithelium (RPE).[40] A2PE is then hydrolyzed to A2E, a major toxic component and photosensitizer of RPE lipofuscin that is increased in *Abca4* KO mouse model.[11,22] LC-HRMS offers the most effective approach for retinoid detection in terms of sensitivity, specificity, and definite mass identification (Figure 3A).[41] To further verify this approach we measured in parallel the bisretinoid levels in eye-cups taken from the *Abca4*KO mouse model at ten weeks of age and find a 3-fold increase relative to the wild-type controls in agreement with that described to date (Figure S5). The *Abca4*$^{Ex42-/-}$ rat shows a 3.5-fold relative increase in A2E at 3 months (Figure 3B) a differential increase that is maintained at 15 months of age (Figure 3E). While A2E accumulates in the RPE, at least 20 bisretinoids emerge earlier in the synthetic cascade and within the POS; while many have been characterized there are countless more potential configurations and transformations. We find a 6-fold increase in the level of one such early precursor A2GPE (Figure 3C,F), a difference that remains stable as the rats age. While the most abundant primary amine in the retina is PE, retinal can technically dimerize upon any primary amine with the rate-limiting step simply being the rearrangement of the Schiff base to a nucleophillic reactive intermediate.[42] In particular, dimerization upon lysine residues of opsin has been described with deamination of the neutral dimer from this reaction resulting in the *at*RAL dimer (dATR).[43,44] The level of dATR is found in excess in the *Abca*$^{Ex42-/-}$ eyes (Figure 3D). Unlike A2E and A2GPE the difference in the


(A)
Abca4wt/wt
Abca4-/-
ONL thickness (µm)
110
90
70
50
n=9
n=7
n=5
n=8
n=5 *
3
6
9
12
15
Months
POS
ONL
GCL


(B)
ONL count
Number of nuclei
50
40
30
20
10
0
****
wt/wt
Abca4Ex42-/-
Abca4wt/wt
Abca4Ex42-/-
POS
ONL
GCL


(C)
a-wave Rod ERG
b-wave Rod ERG
a-wave amplitude (µV)
b-wave amplitude (µV)
40
20
0
160
120
80
40
0
3 mo
6 mo
9 mo
12 mo
Abca4+/+
Abca4ex42-/-


(D)
a-wave Rod/Cone ERG
b-wave Rod/Cone ERG
a-wave amplitude (µV)
b-wave amplitude (µV)
150
100
50
0
320
280
240
200
3 mo
6 mo
9 mo
12 mo
Abca4+/+
Abca4ex42-/-

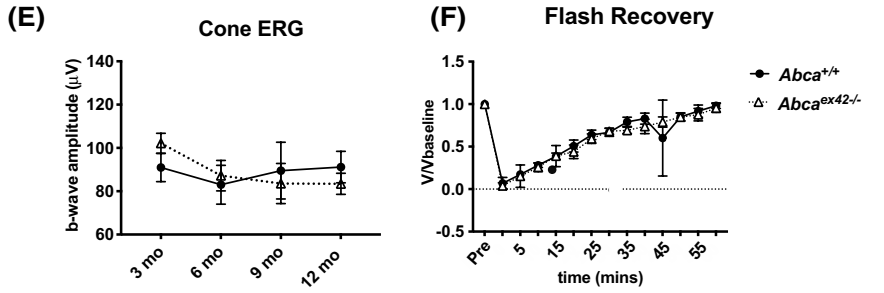

(E)
Cone ERG
b-wave amplitude (µV)
140
120
100
80
60
3 mo
6 mo
9 mo
12 mo
(F)
Flash Recovery
V/Vbaseline
1.5
1.0
0.5
0.0
-0.5
Pre
5
15
25
35
45
55
time (mins)
Abca+/+
Abcaex42-/-

FIGURE 2 Reduced ONL thickness in ABCA4 knockout rats with no change in ERG. (A) OCT measurements of retinal thickness with age were taken of segmented mid-peripheral regions at a fixed distance from the optic nerve as shown in the fundus/OCT image on the right. A 28% thinning of the ONL thinning for the $Abca4^{Ex42-/-}$ retinas is measured by 12 months of age with statistical significance assessed by repeated measures ANOVA (*$p < .05$), $n = 5$. (B) ONL thinning is confirmed by nuclei counting of counter-stained paraffin-embedded retinal sections from rats at 12 months of age, scale bar, 50 μm $n = 3$. (C) Amplitude responses to flash ERG were recorded between $Abca4^{+/+}$ WT (o) and $Abca^{Ex42-/-}$ KO (Δ) rats as they aged. Rod a-wave and b-wave amplitudes show no significant loss in rod sensitivity with age in response to −2.0 Log cd s/m^2 flash, $n = 5$ (data presented as mean values ± SD). (D) The mixed rod-cone a-wave and b-wave amplitudes of $Abca4^{Ex42-/-}$ rats drop significantly with age compared to $Abca4^{+/+}$. Fitting a regression line on the data sets show significant deviation from 0 only for the $Abca4^{Ex42-/-}$ slope, (*$p < .05$) $n = 5$. (E) The cone ERG as determined by photopic flash show no significant differences in the age-related decline of amplitude, $n = 5$ (data presented as mean values ± SD). (F) Dark adaptation kinetics show no differences in dark adaptation response times between $Abca4^{+/+}$ and $Abca4^{Ex42-/-}$ at 6 months of age, $n = 3$. ERG, electroretinogram; GCL; ganglion cell layer; INL, inner nuclear layer; OCT, optical coherence tomography; ONL, outer nuclear layer; POS, photoreceptor outer segment

levels increases further as the rats age, remaining highly significant despite inter-individual variation (Figure 3G). We used a standard curve generated with a stock of synthetic purified A2E to determine the absolute amounts of A2E in the rat eyes (Figure S3). We find 24 pmoles of A2E per eye in the WT while it reaches 81 pmoles/eye in the KO at 3 months of age (Figure 3H). A2E is an important toxic component of the 'flecks' of lipofuscin seen in the STGD1 fundus. Such flecks are evident as increased Fundus autofluorescence (FAF) in patients and in animal models of macular degeneration. The level of FAF is not easily quantifiable requiring quantification targets and an internal calibrator for accurate assessment.[31] To assess the level of autofluoresence and how it correlates with bisretinoid measures we adapted a simplified approach as used on the *Abca4*KO mouse by taking the gray level pixel value in a segmented midperipheral region flanking the optic nerve. All rats born in the colony during the study were passed by this analysis. From this we find an absolute increase in FAF of 24% across the retinas of the $Abca^{Ex42-/-}$ rat at 3 months of age (Figure 3H).

3.3 | Effect of overexpression of retinol dehydrogenase enzymes on $Abca4^{Ex42-/-}$ retinas

Limiting the window in which unbound retinal remains reactive may reduce the level of bisretinoids and their detrimental effect on the retina. The retinally expressed RDH8 and RDH12 retinol dehydrogenase enzymes reduce retinal to the less reactive retinol. We tested the effects of AAV-mediated gene expression of RDH enzymes in the rat $Abca4^{Ex42-/-}$ retina to examine the impact on bisretinoid levels. RDH does not have access to the lumen of the POS where, in the absence of the ABCA4 transporter, dimers of *at*Ral can form in abundance; however increasing the levels of RDH in the cytosol may enhance the rate at which retinal is reduced when present on the cytosolic side before it can diffuse to the lumen and form reactive products. RDH12 for instance, has been shown to be protective against light-induced degeneration in mice.[45] The enzymatic activities of RDH8 or RDH12 may be illustrated as in Figure 4A (adapted from the fluorescent imaging work of Adler and colleagues).[45] The RDH8 construct carries an outer-segment targeting motif while RDH12 is localized to the inner segment and cell body (Figure 4B). Both RDH8 and RDH12 enzymes rely on the cofactor NADPH for functionality creating a distinct NADPH concentration gradient with highest levels at the cell body and inner segment where it can serve as cofactor for RDH12 while the lowest levels are at the tips of the POS.[46] As RDH is a small gene, it fits readily between the ITRs of AAV allowing for expression of RDH8 and RDH12 cDNAs when cloned in an AAV cassette with the rod-specific Rhodopsin kinase (RK) promoter (Figure 4B). An AAV5 carrying the RK promoter but not expressing any protein (AAV-Ctrl) serves as an additional control. The AAVs were subretinally injected into one eye of each animal at approximately 4×10^9 total vector genomes *per* eye. The high expression of the human RDH transgenes in the eyes does not change the expression levels of endogenous rat *Rdh8* and *Rdh12* (Figure 4C). A snapshot by mass spectrometry of the retinal profile in the eyes injected with AAV-hRDH12 show a 2-fold increase in the *ratio* of retinol to retinal in the RPE suggesting that the excess RDH in one eye is reducing the relative level of *at*RAL that accumulates in the RPE relative to the contralateral eye (Figure 4D).

The $Abca^{42-/-}$ rats were injected for each construct in two series of injections. From the first series, 7 rats were injected at 3 months of age and assigned for mass spectrometry analysis. In a second series 5 rats were injected at 6 months of age and the retinas used for imaging and in qPCR analysis. Only rats that showed a normal fundus prior to injection were used for the experiments and all were sacrificed at 3 months after injection. Eye-cups from rats injected with AAV-Ctrl, AAV-hRDH8 or AAV-hRDH12 were analysed by LC-HRMS to obtain a quantitative measure of the autofluorescent bisretinoids. The relative levels of A2E were shown to be unchanged by subretinal injection of AAV-Ctrl or of saline (Figure 5A).

By contrast, the levels of A2E and A2GPE were reduced by 32% compared to the contralateral eye for RDH8 vector injection (Figure 5B,E) while the levels for RDH12 were determined to be 42% reduced (Figure 5C,F). This drop between the injected and contralateral eyes was only significant for the RDH12 group. However, ANOVA analysis between the groups shows the percentage drop across all the treated eyes is not significant (Figure 5D).

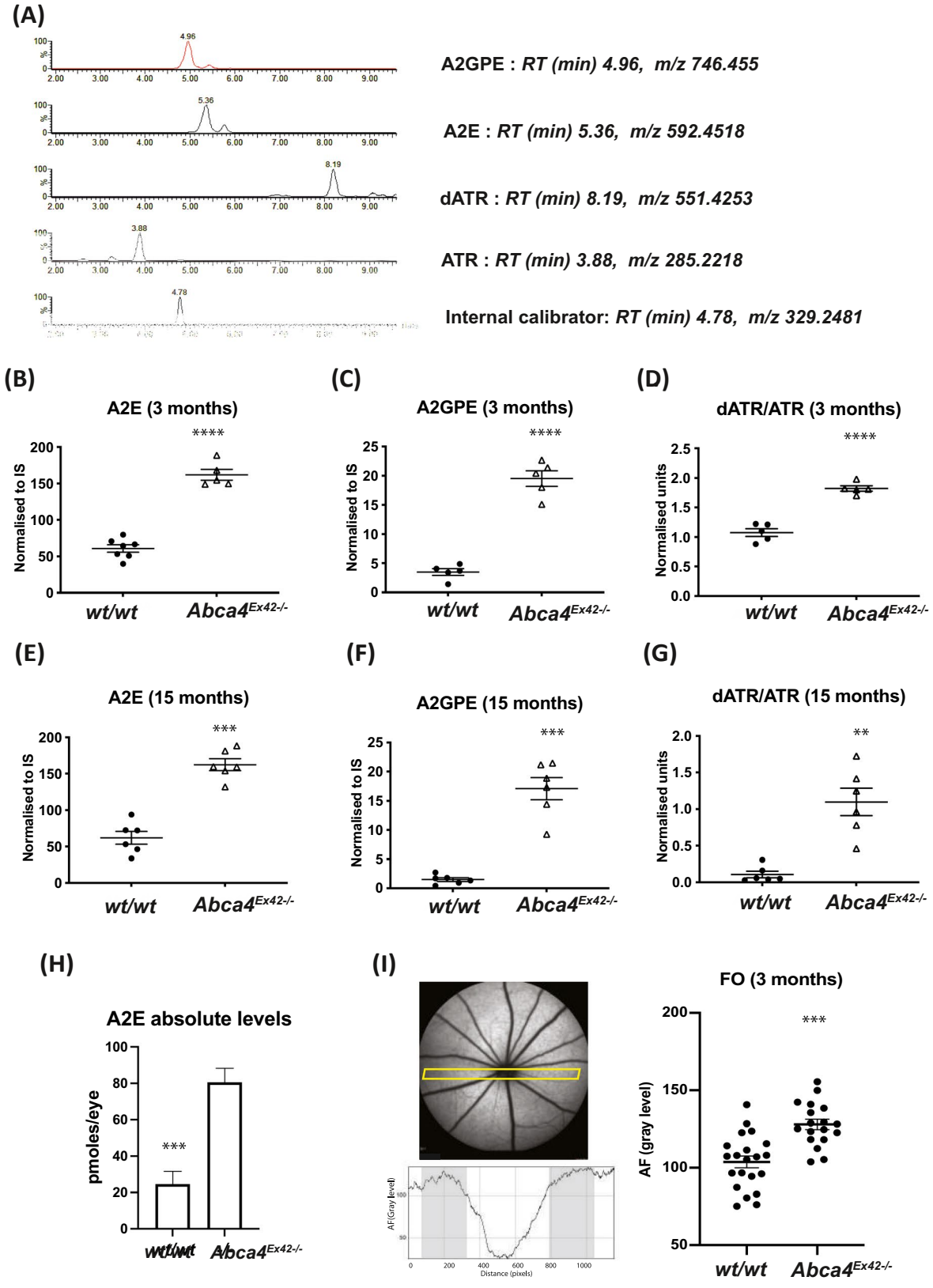


FIGURE 3 Fundus imaging (FO) and bisretinoid levels measured by LC-HRMS analysis of eye-cups of *Abca4*$^{Ex42-/-}$ rats compared to age-matched sibling controls. (A) The retention times and mass/charge ratios of the analyte peaks that are described for this model are shown. This includes A2E, A2GPE, ATR (*at*RAL), dimers of ATR (*at*RAL) and the retinyl acetate used as internal standard (IS) to normalize for the extraction procedure between samples. (B) A2E shows a 3-fold increase in *Abca4*$^{Ex42-/-}$ rats at 3 months, (****$p < .0001$) $n = 5$. (C) A2GPE is increased 6-fold at 3 months, (****$p < .0001$) $n = 5$. (D) The ratio of *at*Ral dimer (dATR) to *at*Ral monomers (ATR) is increased 1.8-fold at 3 months, (****$p < .0001$) $n = 5$. (E) A2E is 3-fold increased in *Abca4*$^{Ex42-/-}$ rats at 15 months (***$p < .001$), $n = 6$. (F) A2GPE levels are increased 11-fold at 15 months (***$p < .001$), $n = 6$. (G) The ratio of *at*Ral dimer (dATR) to *at*Ral monomers (ATR) is increased 10-fold at 15 months, (**$p < .001$) $n = 6$. (H) The absolute levels of A2E in the rat eye-cups at 3 months of age was determined according to the standard curve for synthetic A2E, and shows on average 24 pmole per eye for WT and 81 pmole per eye for *Abca4*$^{Ex42-/-}$ rats, $n = 5$. (I) Representative unprocessed fundus (FO) retinal images used for quantification with the region of interest (ROI) for quantification boxed in yellow. Further selection of two regions at pixel windows of approximately 100–300 and 800–1000 microns around the optic nerve allow for quantification of gray levels in each mid-peripheral region. A histogram of this profile plot for the ROI is shown below this fundus image. Retinal autofluorescence is 24% increased in the *Abca4*$^{Ex42-/-}$ group at 3 months of age. Data were analyzed using Student's *t*-distribution test (***$p < .001$) $n = 18$. A2E, N-retinylidene-N-retinylethanolamine; A2GPE, A2-glycerophosphoetahnolamine; ATR, all-trans retinal; dATR, dimers all-trans retinal; FO, fundus; IS, Internal Standard

It is concluded that the overexpression of RDH enzymes is not having a consistent effect in reducing the bisretinoid levels when unilaterally injected.

3.4 | RDH overexpression and retinal thinning

In the first series of injections ERGs were recorded from injected *Abca4*$^{Ex42-/-}$ rats 1 week before injection when the rats were 3 months of age and 3 months post-injection just prior to sacrifice. These measurements do not show significant changes in wave amplitude of the scotopic (rod) ERG, mesopic (rod-cone) and photopic (cone) conditions recorded post-injection for either groups compared to the control injected group (Figure 6A). A second series of injections was also carried out in older animals at 6 months of age to evaluate any transgene-related toxicity that could result in loss of retinal tissue. The retinal thickness was quantified in vivo at 1 week prior to injection and approximately 3 months post-injection by OCT scanning over the superior peripheral retina where the injection is carried out (Figure 6B). The retinal location at a fixed inferior angle to the injection site was scanned pre- and post-injection. The baseline we expect for thinning of the entire retina during this three month period is no more than 7% (as shown in the control of Figures 2A and 6D). We find a 2.5-fold increase in thinning for hRDH8-injected *Abca*$^{Ex42-/-}$ rats compared to controls (uninjected and injected with an AAV5 not expressing any protein, AAV-Ctrl) (Figure 6D). Vitreous immune infiltrates were not detected in the OCT scans, though such immune cells may already have been cleared out by this 3 month time-point. Despite overall thinning, retinal structure in paraffin-embedded sections is found to be conserved (Figure 6D). Maeda et al. have proposed that the kinetics of the reduction of *at*Ral to *at*Rol is limited by the availability of NADPH rather than by the RDH enzyme itself.[46,47] If RDH8 overexpression depletes the available NADPH in the POS than it may result in POS collapse and RPE atrophy. RDH12 on the other hand is expected to deplete levels of NADPH to a lesser degree as its slower kinetics and the abundance of mitochondria in the cell body ensure greater local availability of NADPH.

For some preliminary insight into these effects we looked at the differential expression of key genes that regulate the ready supply of NADPH in the oxidative branch of the pentose phosphate pathway.[48] By examining gene expression from retinal RNA of rats injected with 4×10^9 total vector genomes of AAV-RDH we find an upregulation of *Pfkm1*, *Taldo1* and *Tkt* in AAV-RDH12 retinas but not in AAV-RDH8 retinas (Figure S6). Adapting the transcriptional program to meet metabolic demands may help the retina meet the demands of the dehydrogenase enzyme. NADPH depletion may nonetheless contribute to the retinal degeneration observed in RDH8-injected *Abca4*$^{Ex42-/-}$ retinas.

4 | DISCUSSION

The suddenness of vision loss often in the teenage years makes STGD1 a particularly devastating form of blindness and has been a high priority for biomedical research in retinal dystrophy. It has been demonstrated that the level of vitamin A dimerization in the retina predicts the progression of the disease. As such, despite the limited number of informative functional models, the testing of potential therapeutics has been feasible in the *Abca4*$^{-/-}$ mouse by using retinoid biochemistry as a biomarker.[24,26,27,49] The need for additional models to test STGD1 therapies led us to develop rat models of STGD1 that are more amenable to stereotactic injection, long-term imaging and immunogenicity studies. In the model described here the deletion of one small exon

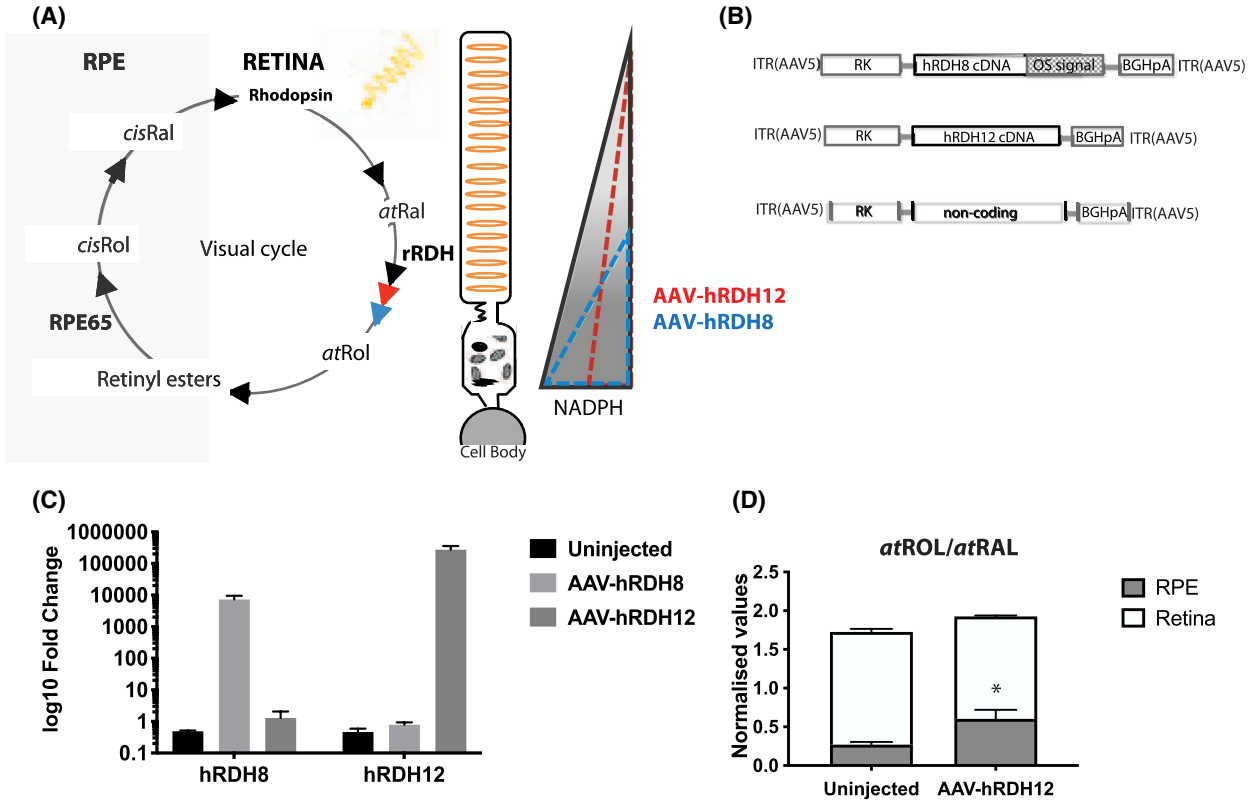


FIGURE 4 RDH expression following subretinal injection of hRDH transgenes in *Abca4*$^{Ex42-/-}$ KO rats. (A) Schema of the visual cycle with the position of rat Retinol Dehydrogenase (rRDH) represented by a black arrow and the transgenic expression of human RDH (AAV-hRDH8 and AAV-hRDH12) represented by blue and red arrows. In theory, by supplementing the enzymatic capacity for the reduction step, the excess *at*Ral that accumulates in the absence of ABCA4 may be more rapidly processed before getting trapped in the outer segment lumen. The shaded triangle to the right shows the NADPH concentration gradient with decreasing levels from the cell body to the outer segment of photoreceptors (adapted from Adler et al.[46]). Overexpression of RDH8 may be expected to cause NADPH levels to be more depleted in the outer segment where RDH8 activity is post-translationally directed. Overexpression of RDH12 may be expected to cause NADPH levels throughout the photoreceptor to be partially depleted. (B) AAV5-based constructs used to express hRDH8 (AAV-hRDH8) and hRDH12 (AAV- hRDH12), as well as a non-expressing AAV5 control (AAV-Ctrl) that were injected subretinally into *Abca4*$^{Ex42-/-}$ rats in this study. (C) Levels of expression from the AAVs are evaluated by RT-qPCR on retinal lysate RNA from subretinally injected *Abca4*$^{Ex42-/-}$ rats compared to uninjected rat retinas, $n = 3$. (D) The levels of *at*Ral and *at*Rol between retina and RPE were evaluated by LC-HRMS analysis from *Abca4*$^{Ex42-/-}$ rats injected with AAV-hRDH12, and the ratio *at*ROL/*at*RAL evaluated for injected versus the non-injected contralateral eye, (*$p < .05$) $n = 3$. A2E, N-retinylidene-N-retinylethanolamine; atRAL, all-trans retinal; atROL, all-trans retinol; LE, left eye; m.p.i., months post-injection; NI, not injected; RDH, retinol dehydrogenase; RE, right eye; RK, rhodopsin kinase

preceding the NBD2 region of the *Abca4* gene led to loss of protein with a subsequent impact on the visual cycle. It was a surprise that this small deletion should lead to such dramatic reduction in protein. Common human mutations in this region, such as G1961E and L1971R are associated with mild to moderate forms of macular degeneration.[50] However, mutations within the NBD2 domain of a number of ABCA transporters have been shown to drastically reduce protein levels when expressed in Cos7 cells with calnexin staining showing that these mutants are highly misfolded and retained in the ER. This may also be the case for the Abca4 knockdown model described here as the residual protein in the mutant rat retina is largely retained in the cytosol.[34,51] In phenotyping, we use the template proposed by Wilner in 1984 in which the validity of an animal model for a disease is assessed by three criteria: Face, Construct and Predictive validity.[29] This rat model does not meet the criterion of face validity, meaning representation of the symptoms described in patients, as a functional phenotype is not manifest in the rat (a limitation likely true for any model lacking a macula). The criterion of construct validity, reflecting pathophysiology, is valid, as the changes in the bisretinoid profile of this rat model are indicative of the pathophysiological change that occurs in STGD1 disease. The predictive validity of this model was finally tested by examining the effects of enhanced expression of retinol dehydrogenase enzymes on the level of bisretinoids. It was previously shown that knocking out both ABCA4 and

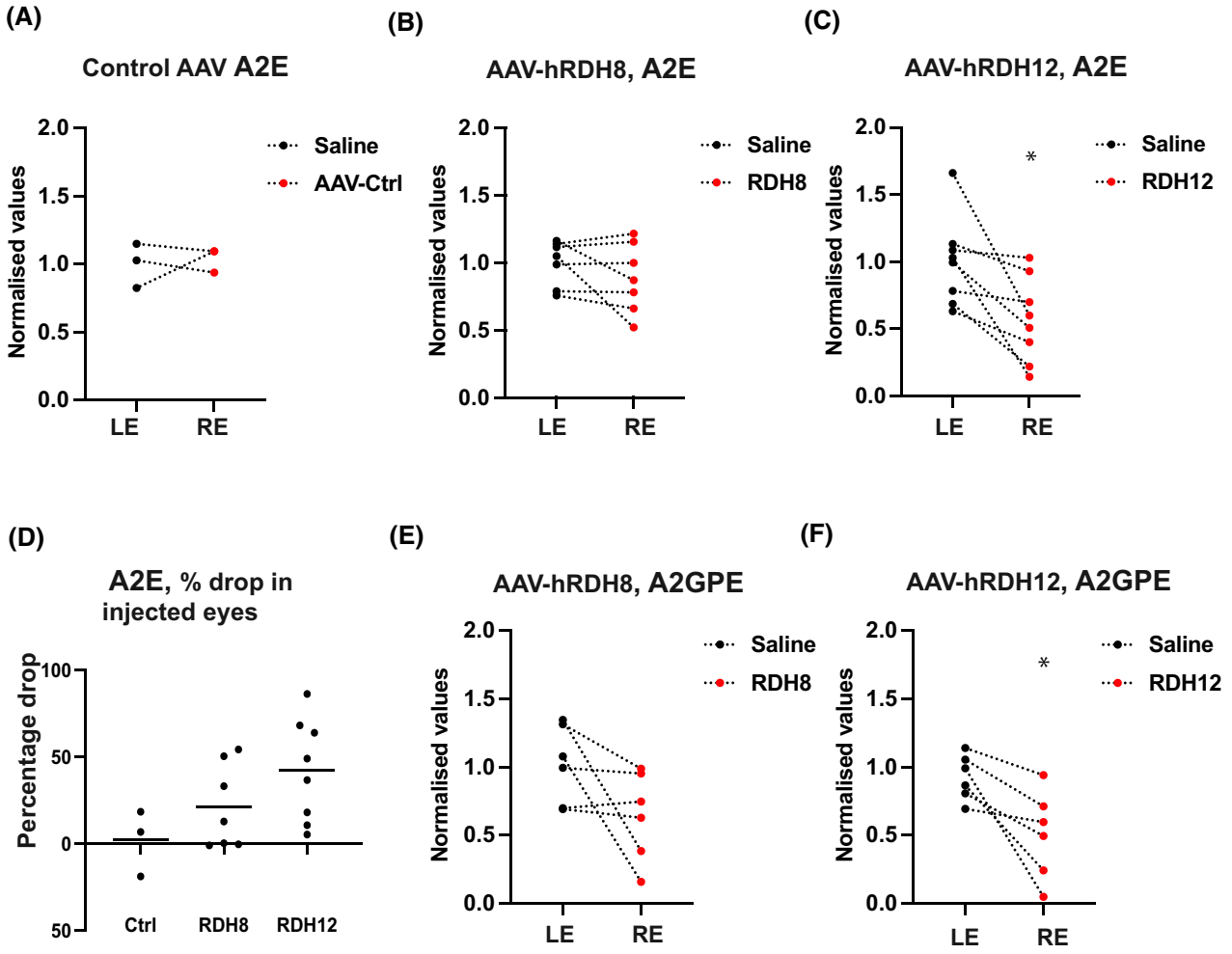
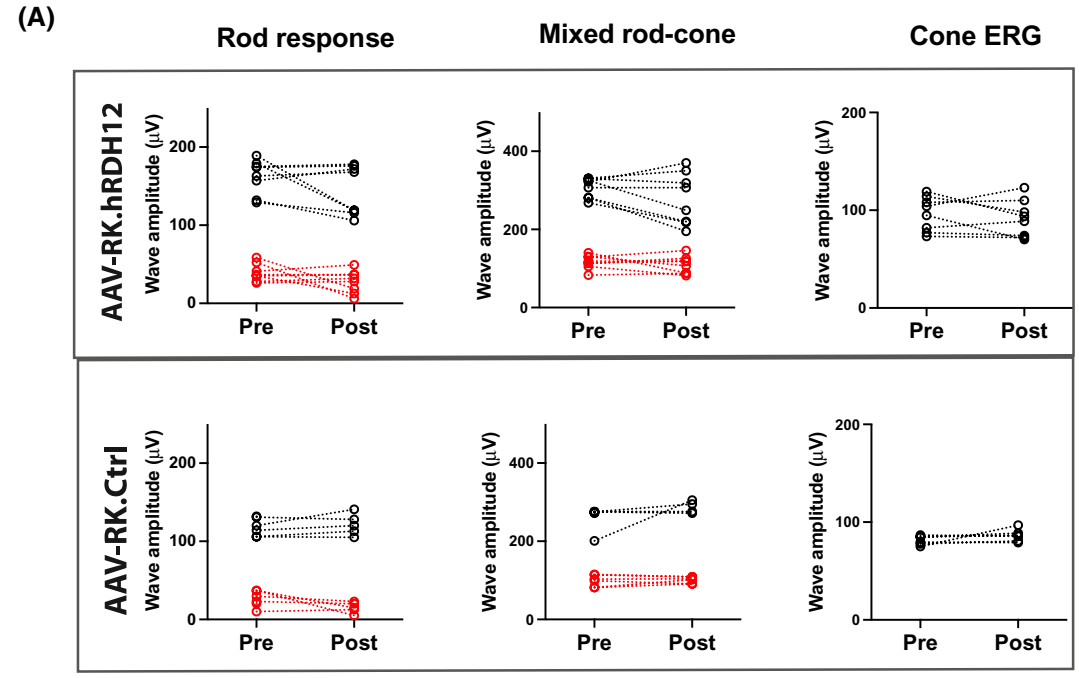
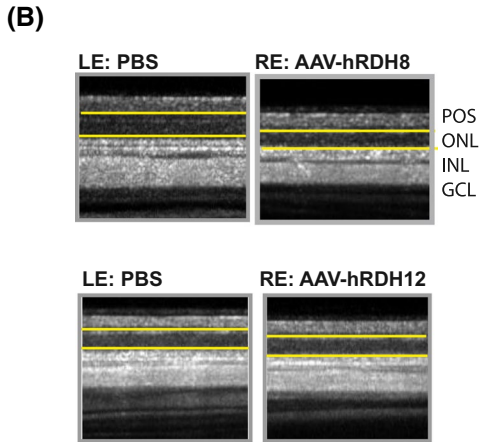


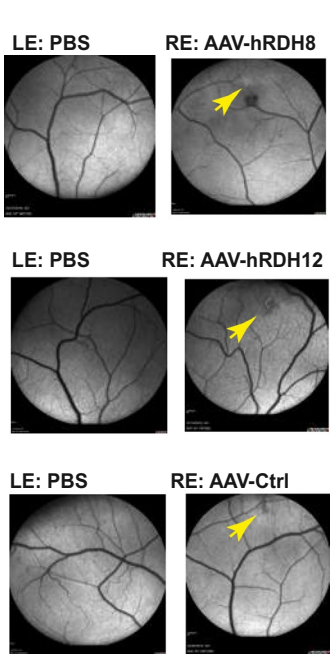
FIGURE 5 Subretinal unilateral injection of hRDH transgenes alters bisretinoid levels in eyes of ABCA4 knockout rats. (A) *Abca4*$^{Ex42-/-}$ rats at 3 months of age were injected in one eye with an AAV5-RK-Control plasmid (AAV-Ctrl) carrying a non-coding transgene under the rhodopsin kinase promoter. The level of A2E was measured in these eyes compared to non-injected contralateral eyes at 3 m.p.i. No significant difference was found between the eyes ($n = 3$). (B) *Abca4*$^{Ex42-/-}$ rats injected with 4×10^9 total vector genomes of AAV5-RK.hRDH8 show a 32% average decrease in levels of A2E at 3 m.p.i. compared with sham-injected contralateral eyes, $n = 7$. (C) *Abca4*$^{Ex42-/-}$ rats injected with 4×10^9 total vector genomes of AAV5-RK.hRDH12 show a 42% average decrease in levels of A2E at 3 m.p.i. compared with sham-injected contralateral eyes, (*$p < .05$ by paired two-tailed t test) $n = 7$. (D) The percentage drop of A2E in the injected eyes of the rats is determined for each group. Variance across the groups is not significant. (E) *Abca4*$^{Ex42-/-}$ rats injected with 4×10^9 total vector genomes of AAV5-RK.hRDH8 show a 34% average decrease in levels of A2GPE at 3 m.p.i. compared with sham-injected contralateral eyes, $n = 7$. (F) *Abca4*$^{Ex42-/-}$ rats injected with 4×10^9 total vector genomes of AAV5-RK.hRDH12 show a 41% average decrease in levels of A2GPE at 3 m.p.i. compared with sham-injected contralateral eyes, (*$p < .05$ by paired two-tailed t test) $n = 7$. A2E, N-retinylidene-N-retinylethanolamine; A2GPE, A2-glycerophosphoetahnolamine; atRAL, all-trans retinal; atROL, all-trans retinol; ctrl, control; LE, left eye; m.p.i., months post-injection; NI, not injected; RDH, retinol dehydrogenase; RE, right eye; RK, rhodopsin kinase

RDH8 in the mouse retina produces severe retinal toxicity and the loss of either results in an increase in bisretinoid levels in mice.[46] With this in mind we examined whether accelerating the reduction of retinal to retinol by supplementing RDH levels might maintain the level of vitamin A dimer below a threshold of toxicity.

While the RDH enzyme is reliant on the ABCA4 flippase to relocate its substrate *at*RAL(-PE) to the cytosolic side for reduction[54] the retinal will itself naturally diffuse in and out of the segments and it can be randomly relocated by both opsin as well as the PE phospholipid which has its own basal rate of flipping. This offers a window of opportunity for RDH to reduce retinal even in the absence of the active retinal relocation by ABCA4. RDH8 overcomes steric volume exclusion in the disc membranes by having a C-terminal POS localizing signal that actively directs it to the outer segment.[55,56] This domain is not present in RDH12 meaning that this enzyme remains in the inner segment and cell body. In the *Abca4*$^{Ex42-/-}$ rat model we find that RDH8 supplementation can reduce


(A)
Rod response
Mixed rod-cone
Cone ERG
AAV-RK.hRDH12
AAV-RK.Ctrl
Wave amplitude (μV)
Pre
Post


(B)
LE: PBS
RE: AAV-hRDH8
LE: PBS
RE: AAV-hRDH12
POS
ONL
INL
GCL


(C)
LE: PBS
RE: AAV-hRDH8
LE: PBS
RE: AAV-hRDH12
LE: PBS
RE: AAV-Ctrl

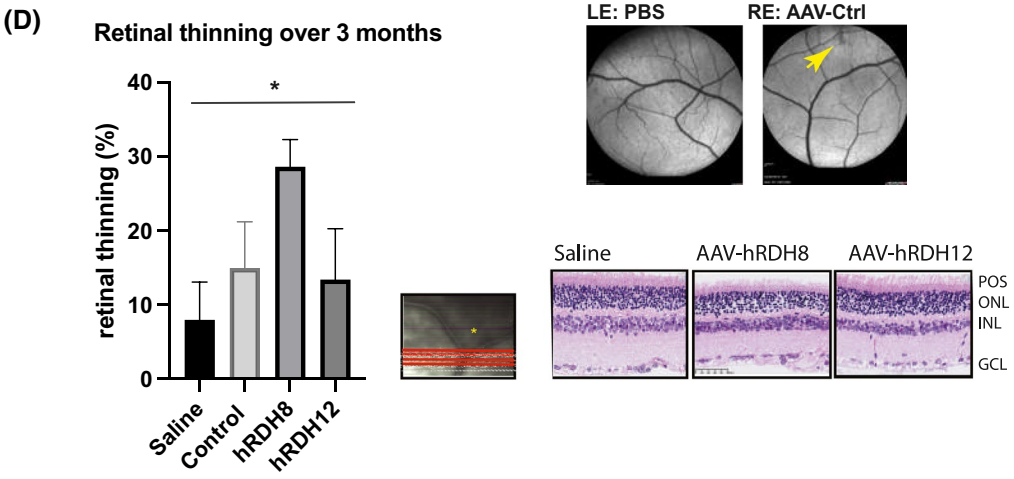

(D)
Retinal thinning over 3 months
retinal thinning (%)
*
Saline
Control
hRDH8
hRDH12
Saline
AAV-hRDH8
AAV-hRDH12
POS
ONL
INL
GCL

FIGURE 6 Impact of hRDH overexpression on retinal structure and function. (A) Pre-injection and post-injection ERGs were recorded from $Abca4^{Ex42-/-}$ rats injected unilaterally with 4×10^9 total vector genomes of vectors expressing RDH12 (AAV-RK.hRDH12 upper panel), $n = 7$ or a control non-expressing transgene (AAV-RK. Ctrl lower panel), $n = 5$. The red line represents the ERG a-wave and the black line represents the b-wave. No significant drop in amplitude was observed post-injection compared to the control condition. (B) OCT scans of injected retinas are shown with the measured ONL highlighted between yellow lines. (C) Representative fundus images of injected rats are shown. $Abca4^{Ex42-/-}$rats injected unilaterally with AAV5-RK.hRDH8 show localized dark scarring and hemorrhage on autofluorescence imaging. This patching is less evident in and AAV5-RK.hRDH12 injected $Abca4^{Ex42-/-}$ rats (middle fundus images) and in retinas receiving an AAV5 control vector (lower fundus images). Yellow arrows show the injection site. (D) The overall retinal thinning was compared between uninjected rats and injected rats for OCT measurements taken at 6 months of age just prior to injection and again 3 months later. The fundus image to the right of the bar graph shows the region that is scanned. For pre- and post-injection comparisons the scans are at a fixed location (marked by red lines) in the peripheral superior retina just below the injection site (marked by a yellow asterix). A 2.5-fold increase in thinning across the span of the retina is found for hRDH8 injected rats compared to uninjected or hRDH12-injected rats, $n = 5$ ($p < .05$). To the right of the fundus scanned image are paraffin-embedded, HNE counter-stained retinal sections showing that despite thinning overall retinal structure is conserved in the injected rats

A2E levels by 32% while RDH12 causes a 42% average drop between injected and contralateral uninjected eyes. At the same time signs of retinal degeneration are evident by fundus imaging at 3 months post-injection, specifically in the RDH8-injected retinas. No fundus changes were observed in rats subretinally injected with equivalent volume and serotype of AAV carrying the RK promoter and a null-expressing transgene (AAV-Ctrl). However, an alternative control vector carrying a mutant non-expressing RDH transgene would be more suited to determine whether ONL degeneration is due to RDH enzymatic activity and not simply sequence-specific effects of the vector. The rate kinetics of the RDH8-mediated reduction of *at*Ral is significantly higher than the RDH12-mediated reduction and is estimated to account for 70% of the total enzyme activity generating *at*RAL in mouse rod photoreceptors.[47,52,53] Cellular degeneration as suggested by fundus and OCT analysis of RDH8-injected retinas is potentially due to the active RDH enzyme depleting stocks of outer segment NADPH levels. NADPH is essential for a number of reductive biosynthetic reactions in the photoreceptor cell, including the ribonucleotide and fatty acid biosynthesis needed for membrane turnover so it may be expected that NADPH loss in the POS would ultimately cause outer segment collapse and subsequent cell loss. From this study we cannot ascertain whether the reduction of bisretinoid levels in RDH8-injected eyes is simply a consequence of overall outer segment loss due to degeneration or is really due to changes in retinoid cycling. For RDH12 on the other hand OCT imaging as well as ERG suggests these retinas remain healthy. The reduction in bisretinoid levels warrants further investigation of RDH enzymes to modulate the Stargardt phenotype as has been proposed by others.[57] However, we cannot conclude efficacy from this study and have recorded the potential for toxicity when RDH8 is over-expressed.

With much of its pathophysiology unraveled, research into STGD1 has of late been more actively focused on therapy. As it is a macular disease there is little availability of suitable animal models containing sufficiently dense cone-rich area in which to test functional rescue. Recently a Labrador retriever disease model carrying a premature stop codon in exon 28 of the canine ABCA4 gene and showing some cone dysfunction was described and may support large animal studies.[58] In the meantime, therapies can be efficiently screened in rodent models such as the new rat model described here using bisretinoid biomarkers as the criteria for evaluation of therapeutic directions.

ACKNOWLEDGMENTS

We thank Séverine Remy, Laurent Tesson and Ignacio Anegon of the rat transgenesis platform (Biogenouest). We are also grateful to the Biogenouest Corsaire core facility for their financial support in mass spectrometry analyses. We thank the Nantes Vector Core Facility (UMR1089 CPV, https://umr1089.univ-nantes.fr/facilities-cores/) for producing the rAAV vectors and Philippe Hulin (Cellular and Tissue Imaging Core Facility, INSERM, Nantes, France) for their technical assistance. We are very grateful to the staff of the Boisbonne Center for animal care and for their continuous support during the course of this study. This work was supported by Nantes University, Inserm, the Region Pays de la Loire (Connect Talent, 2015_Gene Therapy for Vision) and Aviesan/UNADEV grant #19UU50 (Development of novel gene therapy strategies for Stargardt Disease).

DISCLOSURES

We have no conflict of interests to declare.

AUTHOR CONTRIBUTIONS

N. Provost and T. Cronin carried out all sample preparation and molecular biology experiments and analysis, C. Audrain cloned AAV constructs, M. Croyal performed mass spectrometry analysis, L. Libeau carried out ERG studies, A. Mendes-Madeira performed the OCT imaging

while V. Pichard and E. Toublanc carried out the OCT analysis, J. B. Ducloyer and A. Mendes-Madeira did the subretinal injections, C. Isiegas and O. Adjali conceived and funded the project while T. Cronin and O. Adjali designed the experiments; T. Cronin and O. Adjali wrote and edited the manuscript.

ORCID

T. Cronin https://orcid.org/0000-0002-2938-2765

REFERENCES

1. Beharry S, Zhong M, Molday RS. N-retinylidene-phosphatidylethanolamine is the preferred retinoid substrate for the photoreceptor-specific ABC transporter ABCA4 (ABCR). *J Biol Chem*. 2004;279(52):53972-53979. doi:10.1074/jbc.M405216200
2. Biswas-Fiss EE. Interaction of the nucleotide binding domains and regulation of the ATPase activity of the human retina specific ABC transporter, ABCR. *Biochemistry*. 2006;45(11):3813-3823. doi:10.1021/bi052059u
3. Sun H, Molday RS, Nathans J. Retinal stimulates ATP hydrolysis by purified and reconstituted ABCR, the photoreceptor-specific ATP-binding cassette transporter responsible for Stargardt disease. *J Biol Chem*. 1999;274(12):8269-8281.
4. Allikmets R, Singh N, Sun H, et al. A photoreceptor cell-specific ATP-binding transporter gene (ABCR) is mutated in recessive Stargardt macular dystrophy. *Nat Genet*. 1997;15(3):236-246. doi:10.1038/ng0397-236
5. Allikmets R, Wasserman WW, Hutchinson A, et al. Organization of the ABCR gene: analysis of promoter and splice junction sequences. *Gene*. 1998;215(1):111-122.
6. Molday LL, Rabin AR, Molday RS. ABCR expression in foveal cone photoreceptors and its role in Stargardt macular dystrophy. *Nat Genet*. 2000;25(3):257-258. doi:10.1038/77004
7. Allikmets R, Shroyer NF, Singh N, et al. Mutation of the Stargardt disease gene (ABCR) in age-related macular degeneration. *Science*. 1997;277(5333):1805-1807.
8. Eldred GE, Lasky MR. Retinal age pigments generated by self-assembling lysosomotropic detergents. *Nature*. 1993;361(6414):724-726. doi:10.1038/361724a0
9. Finnemann SC, Leung LW, Rodriguez-Boulan E. The lipofuscin component A2E selectively inhibits phagolysosomal degradation of photoreceptor phospholipid by the retinal pigment epithelium. *Proc Natl Acad Sci USA*. 2002;99(6):3842-3847. doi:10.1073/pnas.052025899
10. Lakkaraju A, Finnemann SC, Rodriguez-Boulan E. The lipofuscin fluorophore A2E perturbs cholesterol metabolism in retinal pigment epithelial cells. *Proc Natl Acad Sci USA*. 2007;104(26):11026-11031. doi:10.1073/pnas.0702504104
11. Sparrow JR, Fishkin N, Zhou J, et al. A2E, a byproduct of the visual cycle. *Vision Res*. 2003;43(28):2983-2990.
12. The rate of vitamin A dimerization in lipofuscinogenesis, fundus autofluorescence, retinal senescence and degeneration. Accessed January 22, 2020. https://www.ncbi.nlm.nih.gov/pubmed/26427431
13. Vives-Bauza C, Anand M, Shirazi AK, et al. The age lipid A2E and mitochondrial dysfunction synergistically impair phagocytosis by retinal pigment epithelial cells. *J Biol Chem*. 2008;283(36):24770-24780. doi:10.1074/jbc.M800706200
14. Zhou J, Jang YP, Kim SR, Sparrow JR. Complement activation by photooxidation products of A2E, a lipofuscin constituent of the retinal pigment epithelium. *Proc Natl Acad Sci USA*. 2006;103(44):16182-16187. doi:10.1073/pnas.0604255103
15. Washington I, Saad L. The rate of vitamin A dimerization in lipofuscinogenesis, fundus autofluorescence, retinal senescence and degeneration. *Adv Exp Med Biol*. 2016;854:347-353. doi:10.1007/978-3-319-17121-0_46
16. Saari JC. Biochemistry of visual pigment regeneration: the Friedenwald lecture. *Invest Ophthalmol Vis Sci*. 2000;41(2):337-348.
17. Jin M, Yuan Q, Li S, Travis GH. Role of LRAT on the retinoid isomerase activity and membrane association of Rpe65. *J Biol Chem*. 2007;282(29):20915-20924. doi:10.1074/jbc.M701432200
18. Lamb TD, Pugh EN. Dark adaptation and the retinoid cycle of vision. *Prog Retin Eye Res*. 2004;23(3):307-380. doi:10.1016/j.preteyeres.2004.03.001
19. Rattner A, Smallwood PM, Nathans J. Identification and characterization of all-trans-retinol dehydrogenase from photoreceptor outer segments, the visual cycle enzyme that reduces all-trans-retinal to all-trans-retinol. *J Biol Chem*. 2000;275(15):11034-11043. doi:10.1074/jbc.275.15.11034
20. Chen C, Thompson DA, Koutalos Y. Reduction of all-trans-retinal in vertebrate rod photoreceptors requires the combined action of RDH8 and RDH12. *J Biol Chem*. 2012;287(29):24662-24670. doi:10.1074/jbc.M112.354514
21. Parker RO, Crouch RK. Retinol dehydrogenases (RDHs) in the visual cycle. *Exp Eye Res*. 2010;91(6):788-792. doi:10.1016/j.exer.2010.08.013
22. Weng J, Mata NL, Azarian SM, Tzekov RT, Birch DG, Travis GH. Insights into the function of Rim protein in photoreceptors and etiology of Stargardt's disease from the phenotype in abcr knockout mice. *Cell*. 1999;98(1):13-23. doi:10.1016/S0092-8674(00)80602-9
23. Dyka FM, Molday LL, Chiodo VA, Molday RS, Hauswirth WW. Dual ABCA4-AAV vector treatment reduces pathogenic retinal A2E accumulation in a mouse model of autosomal recessive Stargardt disease. *Hum Gene Ther*. 2019;30(11):1361-1370. doi:10.1089/hum.2019.132
24. McClements ME, Barnard AR, Singh MS, et al. An AAV dual vector strategy ameliorates the Stargardt phenotype in adult Abca4$^{-/-}$ mice. *Hum Gene Ther*. 2019;30(5):590-600. doi:10.1089/hum.2018.156
25. Tornabene P, Trapani I, Minopoli R, et al. Intein-mediated protein trans-splicing expands adeno-associated virus transfer capacity in the retina. *Sci Transl Med*. 2019;11(492):15. doi:10.1126/scitranslmed.aav4523
26. Racz B, Varadi A, Kong J, et al. A non-retinoid antagonist of retinol-binding protein 4 rescues phenotype in a model of Stargardt disease without inhibiting the visual cycle. *J Biol Chem*. 2018;293(29):11574-11588. doi:10.1074/jbc.RA118.002062
27. Charbel Issa P, Barnard AR, Herrmann P, Washington I, MacLaren RE. Rescue of the Stargardt phenotype in Abca4 knockout mice through inhibition of vitamin A dimerization. *Proc Natl Acad Sci USA*. 2015;112(27):8415-8420. doi:10.1073/pnas.1506960112
28. Remy S, Chenouard V, Tesson L, et al. Generation of gene-edited rats by delivery of CRISPR/Cas9 protein and donor DNA into intact zygotes using electroporation. *Sci Rep*. 2017;7(1):16554. doi:10.1038/s41598-017-16328-y
29. Willner P. The validity of animal models of depression. *Psychopharmacology*. 1984;83(1):1-16. doi:10.1007/bf00427414
30. Maeda A, Golczak M, Maeda T, Palczewski K. Limited roles of Rdh8, Rdh12, and Abca4 in all-trans-retinal clearance in

mouse retina. *Invest Ophthalmol Vis Sci*. 2009;50(11):5435-5443. doi:10.1167/iovs.09-3944

31. Charbel Issa P, Singh MS, Lipinski DM, et al. Optimization of in vivo confocal autofluorescence imaging of the ocular fundus in mice and its application to models of human retinal degeneration. *Invest Ophthalmol Vis Sci*. 2012;53(2):1066-1075. doi:10.1167/iovs.11-8767
32. Pfaffl MW. A new mathematical model for relative quantification in real-time RT-PCR. *Nucleic Acids Res*. 2001;29(9):e45.
33. Fujinami K, Strauss RW, Chiang J-W, et al. Detailed genetic characteristics of an international large cohort of patients with Stargardt disease: ProgStar study report 8. *Br J Ophthalmol*. 2018. doi:10.1136/bjophthalmol-2018-312064
34. Molday LL, Wahl D, Sarunic MV, Molday RS. Localization and functional characterization of the p.Asn965Ser (N965S) ABCA4 variant in mice reveal pathogenic mechanisms underlying Stargardt macular degeneration. *Hum Mol Genet*. 2018;27(2):295-306. doi:10.1093/hmg/ddx400
35. Pawar AS, Qtaishat NM, Little DM, Pepperberg DR. Recovery of rod photoresponses in ABCR-deficient mice. *Invest Ophthalmol Vis Sci*. 2008;49(6):2743-2755. doi:10.1167/iovs.07-1499
36. Mata NL, Tzekov RT, Liu X, Weng J, Birch DG, Travis GH. Delayed dark-adaptation and lipofuscin accumulation in abcr+/- mice: implications for involvement of ABCR in age-related macular degeneration. *Invest Ophthalmol Vis Sci*. 2001;42(8):1685-1690.
37. Marc RE, Jones BW. Retinal remodeling in inherited photoreceptor degenerations. *Mol Neurobiol*. 2003;28(2):139-147. doi:10.1385/MN:28:2:139
38. Leinonen H, Pham NC, Boyd T, Santoso J, Palczewski K, Vinberg F. Homeostatic plasticity in the retina is associated with maintenance of night vision during retinal degenerative disease. *eLife*. 2020;9. doi:10.7554/eLife.59422
39. Care RA, Anastassov IA, Kastner DB, Kuo Y-M, Della Santina L, Dunn FA. Mature retina compensates functionally for partial loss of rod photoreceptors. *Cell Rep*. 2020;31(10):107730. doi:10.1016/j.celrep.2020.107730
40. Sparrow JR, Kim SR, Cuervo AM, Bandhyopadhyayand U. A2E, a pigment of RPE lipofuscin, is generated from the precursor, A2PE by a lysosomal enzyme activity. *Adv Exp Med Biol*. 2008;613:393-398. doi:10.1007/978-0-387-74904-4_46
41. Gutierrez DB, Blakeley L, Goletz PW, et al. Mass spectrometry provides accurate and sensitive quantitation of A2E. *Photochem Photobiol Sci*. 2010;9(11):1513-1519. doi:10.1039/c0pp00230e
42. Kaufman Y, Ma L, Washington I. Deuterium enrichment of vitamin A at the C20 position slows the formation of detrimental vitamin A dimers in wild-type rodents. *J Biol Chem*. 2011;286(10):7958-7965. doi:10.1074/jbc.M110.178640
43. Fishkin N, Jang Y-P, Itagaki Y, Sparrow JR, Nakanishi K. A2-rhodopsin: a new fluorophore isolated from photoreceptor outer segments. *Org Biomol Chem*. 2003;1(7):1101-1105. doi:10.1039/b212213h
44. Ueda K, Kim HJ, Zhao J, Sparrow JR. Bisretinoid photodegradation is likely not a good thing. *Adv Exp Med Biol*. 2018;1074:395-401. doi:10.1007/978-3-319-75402-4_49
45. Maeda A, Maeda T, Imanishi Y, et al. Retinol dehydrogenase (RDH12) protects photoreceptors from light-induced degeneration in mice. *J Biol Chem*. 2006;281(49):37697-37704. doi:10.1074/jbc.M608375200
46. Adler L, Chen C, Koutalos Y. Mitochondria contribute to NADPH generation in mouse rod photoreceptors. *J Biol Chem*. 2014;289(3):1519-1528. doi:10.1074/jbc.M113.511295
47. Maeda A, Maeda T, Sun W, Zhang H, Baehr W, Palczewski K. Redundant and unique roles of retinol dehydrogenases in the mouse retina. *Proc Natl Acad Sci USA*. 2007;104(49):19565-19570. doi:10.1073/pnas.0707477104
48. Patra KC, Hay N. The pentose phosphate pathway and cancer. *Trends Biochem Sci*. 2014;39(8):347-354. doi:10.1016/j.tibs.2014.06.005
49. Lenis TL, Sarfare S, Jiang Z, Lloyd MB, Bok D, Radu RA. Complement modulation in the retinal pigment epithelium rescues photoreceptor degeneration in a mouse model of Stargardt disease. *Proc Natl Acad Sci USA*. 2017;114(15):3987-3992. doi:10.1073/pnas.1620299114
50. Cella W, Greenstein VC, Zernant-Rajang J, et al. G1961E mutant allele in the Stargardt disease gene ABCA4 causes bull's eye maculopathy. *Exp Eye Res*. 2009;89(1):16-24. doi:10.1016/j.exer.2009.02.001
51. Quazi F, Molday RS. Differential phospholipid substrates and directional transport by ATP-binding cassette proteins ABCA1, ABCA7, and ABCA4 and disease-causing mutants. *J Biol Chem*. 2013;288(48):34414–26. https://doi.org/10.1074/jbc.M113.508812. Epub 2013 Oct 4. PMID: 24097981; PMCID: PMC3843056.
52. Kurth I, Thompson DA, Rüther K, et al. Targeted disruption of the murine retinal dehydrogenase gene Rdh12 does not limit visual cycle function. *Mol Cell Biol*. 2007;27(4):1370-1379. doi:10.1128/MCB.01486-06
53. Maeda A, Maeda T, Golczak M, Palczewski K. Retinopathy in mice induced by disrupted all-trans-retinal clearance. *J Biol Chem*. 2008;283(39):26684-26693. doi:10.1074/jbc.M804505200
54. Quazi F, Lenevich S, Molday RS. ABCA4 is an N-retinylidene-phosphatidylethanolamine and phosphatidylethanolamine importer. *Nat Commun*. 2012;3:925. doi:10.1038/ncomms1927
55. Najafi M, Maza NA, Calvert PD. Steric volume exclusion sets soluble protein concentrations in photoreceptor sensory cilia. *Proc Natl Acad Sci USA*. 2012;109(1):203-208. doi:10.1073/pnas.1115109109
56. Luo W, Marsh-Armstrong N, Rattner A, Nathans J. An outer segment localization signal at the C terminus of the photoreceptor-specific retinol dehydrogenase. *J Neurosci*. 2004;24(11):2623-2632. doi:10.1523/JNEUROSCI.5302-03.2004
57. Bennett J, Sun J, Vasireddy V. Methods and compositions for treatment of disorders and diseases involving rdh12. WO2018009814A1, Jan. 11, 2018. Accessed May 24, 2020. https://patents.google.com/patent/WO2018009814A1/en
58. Mäkeläinen S, Gòdia M, Hellsand M, et al. An ABCA4 loss-of-function mutation causes a canine form of Stargardt disease. *PLoS Genet*. 2019;15(3):e1007873. doi:10.1371/journal.pgen.1007873

SUPPORTING INFORMATION

Additional supporting information may be found online in the Supporting Information section.

How to cite this article: Cronin T, Croyal M, Provost N, et al. Effect of retinol dehydrogenase gene transfer in a novel rat model of Stargardt disease. *FASEB J*. 2021;35:e21934. https://doi.org/10.1096/fj.202002525RRR